Nanoscale Research Letters
a SpringerOpen Journal

NANO EXPRESS Open Access

High breakdown voltage in AlGaN/GaN HEMTs using AlGaN/GaN/AlGaN quantum-well electron-blocking layers

Ya-Ju Lee[1*], Yung-Chi Yao[1], Chun-Ying Huang[2], Tai-Yuan Lin[3], Li-Lien Cheng[1], Ching-Yun Liu[1], Mei-Tan Wang[4] and Jung-Min Hwang[4]

Abstract

In this paper, we numerically study an enhancement of breakdown voltage in AlGaN/GaN high-electron-mobility transistors (HEMTs) by using the AlGaN/GaN/AlGaN quantum-well (QW) electron-blocking layer (EBL) structure. This concept is based on the superior confinement of two-dimensional electron gases (2-DEGs) provided by the QW EBL, resulting in a significant improvement of breakdown voltage and a remarkable suppression of spilling electrons. The electron mobility of 2-DEG is hence enhanced as well. The dependence of thickness and composition of QW EBL on the device breakdown is also evaluated and discussed.

Keywords: AlGaN/GaN HEMT; 2-DEG; Breakdown voltage

Background

GaN-based high-electron-mobility transistors (HEMTs) have attracted considerable interests for the high-speed and high-power-switching applications because of their outstanding electronic properties. The high sheet-carrier density of the two-dimensional electron-gas (2-DEG) [1,2] and large critical breakdown electric field [3,4] allow the fabricated HEMT devices with unprecedented high drain current density and large breakdown voltage, which are essential for the important applications of power devices [5-9]. However, the high sheet electron density inherently in GaN-based HEMTs will inevitably induce the spillover of transport electrons at high-drain-voltage conditions, and that becomes a growing issue. In general, the confinement of transport electrons to the bottom side of the device is insufficient in the conventional AlGaN/GaN HEMT, due mainly to the insufficient potential height provided by the GaN buffer layer underneath. Consequently, transport electrons supposed to be confined within the 2-DEG channel would easily spill or leak into the buffer layer, causing a rapid increase of subthreshold drain leakage currents, accelerating the device breakdown. The above-mentioned phenomenon is often interpreted as the 'punchthrough effect,' hindering the further applications of GaN-based HEMTs. Therefore, methods improving the confinement of transport electrons within the channel layer and alleviating the punch-through effect are necessary. Over the years, several approaches, such as the introduction of p-type doping to the GaN buffer layer [10-12] and the use of AlGaN/GaN/AlGaN double-heterojunction HEMTs [13-15], have been reported to enhance the breakdown voltage of GaN-based HEMTs. The basic principle is to raise the conduction band of the GaN buffer layer, and thus generates a deeper and narrower potential well for the better confinement of 2-DEG.

In this work, we present an improved bottom confinement of 2-DEG by introducing the AlGaN/GaN/AlGaN quantum-well (QW) electron-blocking layer (EBL) structure. It is shown that the large electric field induced at the interfaces of AlGaN/GaN/AlGaN QW EBL effectively depletes the spilling electrons toward the 2-DEG channel. As compared to previous approaches, the subthreshold drain leakage current becomes less sensitive to the drain voltage (V_{ds}), and that postpones the HEMT breakdown. Meanwhile, our proposed structure not only exhibits the highest electron mobility among other compared HEMT devices but also allows a great tolerance for epitaxial

* Correspondence: yajulee@ntnu.edu.tw
[1]Institute of Electro-Optical Science and Technology, National Taiwan Normal University, 88, Sec. 4, Ting-Chou Road, Taipei 116, Taiwan
Full list of author information is available at the end of the article

imperfections during the device fabrication. As a result, we conclude that the proposed AlGaN/GaN/AlGaN QW EBL HEMT is viable and highly promising for the high-speed and high-power-switching applications.

Methods

For comparison, four types of devices were numerically studied and the schematic structures are plotted in Figure 1. All devices are designed on an insulating sapphire substrate and have a 40-nm-thick AlN nucleation layer followed by an un-doped GaN buffer layer with a thickness of 1.5 μm.

For the conventional HEMT, a 45-nm-thick un-doped GaN was employed as the channel layer. To alleviate the 2-DEG spillover, a 10-nm-thick EBL was created by p-type doping ($p = 1 \times 10^{18}$ cm^{-3}) to the bottom region of the GaN channel layer, i.e., structure A. For structure B and structure C, we replaced the original 10-nm-thick GaN EBL with $Al_{0.1}Ga_{0.9}N$ EBL and $Al_{0.1}Ga_{0.9}N/GaN/Al_{0.1}Ga_{0.9}N$ QW EBL, respectively. The dopant polarity and doping concentration for the EBLs of structure B and structure C remain the same as $p = 1 \times 10^{18}$ cm^{-3}. Finally, all structures were capped by an un-doped 20-nm-thick $Al_{0.2}Ga_{0.8}N$ barrier layer. The HEMT dimension is designed as 5.4 μm × 200 μm with a gate length of 0.6 μm for numerical analyzing. Both gate-source and gate-drain distances were set to 1.4 μm. To reduce the complexity of physical simulation of the device, here, we assume that the source and drain metals are the perfect Ohmic contact to the $Al_{0.2}Ga_{0.8}N$ barrier layer, and the gate metal is the ideal Schottky contact. To calculate the performance of the HEMT, we have used the finite element simulation program - APSYS. The electrical property of the HEMT was performed by solving the Poisson's equation and the continuity equation. The transport model of electrons and holes considers their drift and diffusion in the devices. The material parameters used in this work can be found in [16] and the references therein. The bandgap of $Al_xGa_{1-x}N$ as a function of the aluminum composition (x) is given by

$$E_g(x) = 6.13x + 3.42(1-x) - 1.20x(1-x) \text{ eV}. \quad (1)$$

The bowing factor adopted in Equation 1 is $b = 1.20$ eV [17], and the conduction band offset for AlGaN/GaN heterojunction is set to 0.68. The APSYS program employs the $6 \times 6\, k \cdot p$ model to depict the energy band profile for the strained wurtzite structure [18-20]. Both spontaneous and piezoelectric polarizations were considered in the simulations. The spontaneous polarization in c-plane $Al_xGa_{1-x}N$ as a function of aluminum composition (x) is given by [21]

$$P^{sp}_{Al_xGa_{1-x}N}(x) = [-0.090x - 0.034(1-x) + 0.019x(1-x)] \text{ cm}^{-2}, \quad (2)$$

while the piezoelectric polarization of AlGaN pseudomorphically grown on the GaN template is calculated by [22]

$$P^{pz}_{Al_xGa_{1-x}N}(x) = [-0.0525x - 0.0282x(1-x)]\text{cm}^{-2}. \quad (3)$$

In the drift-diffusion simulations of AlGaN/GaN HEMTs, the value of electron mobility is critical to describe the transport behavior of 2-DEG. The electron mobility as a function of the longitudinal electric field in the 2-DEG

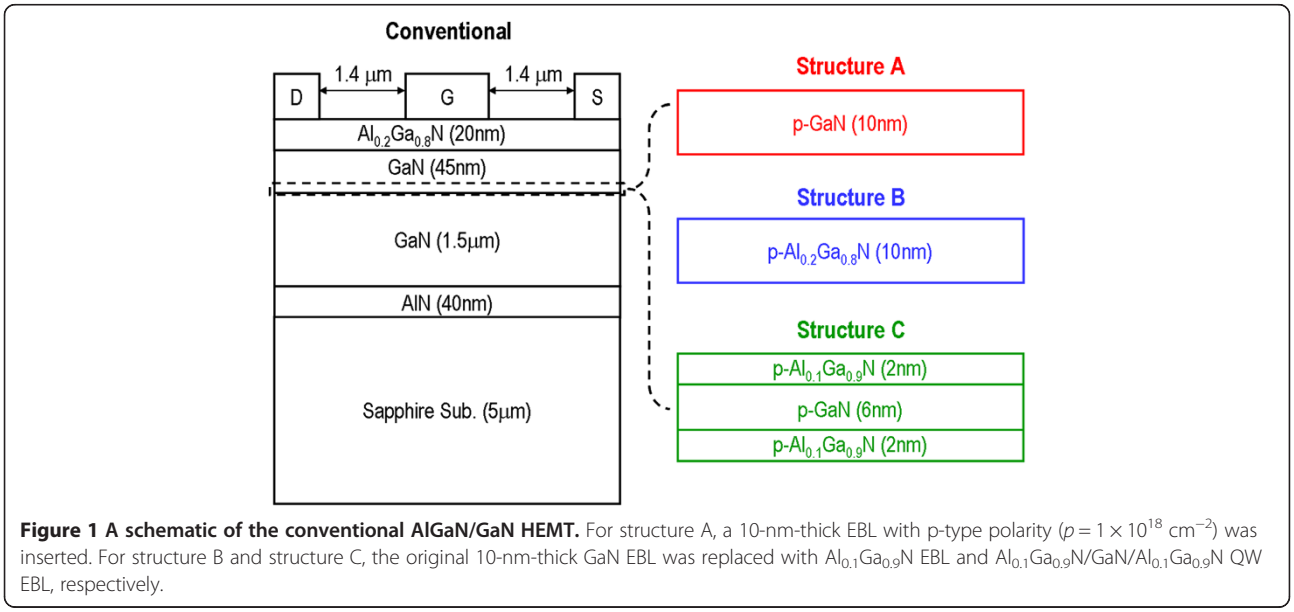

Figure 1 A schematic of the conventional AlGaN/GaN HEMT. For structure A, a 10-nm-thick EBL with p-type polarity ($p = 1 \times 10^{18}$ cm^{-2}) was inserted. For structure B and structure C, the original 10-nm-thick GaN EBL was replaced with $Al_{0.1}Ga_{0.9}N$ EBL and $Al_{0.1}Ga_{0.9}N/GaN/Al_{0.1}Ga_{0.9}N$ QW EBL, respectively.

channel, $\mu_n(E)$, is assumed to follow the Caughey and Thomas model given by [23]

$$\mu_n(E) = \mu_{n0}\left[1 + \frac{\mu_{n0}E}{v_{\text{sat}}}\right]^{-1/\beta_n} \text{ cm}^2/\text{V-s} \quad (4)$$

where μ_{n0} is the low-field electron mobility, v_{sat} is the saturated value of the electron velocity, and β_n is a fitting parameter. To increase the accuracy of the calculation for the breakdown voltage and near-breakdown behavior of the HEMT, it is necessary to include the impact ionization. The generation rate of electron-hole pairs due to impact ionization is given by [24]

$$G = \alpha_n \frac{J_n}{q} + \alpha_p \frac{J_p}{q} \quad (5)$$

where α_n and α_p are the electron and hole ionization rate defined as the number of electron-hole pairs generated by an electron per unit distance traveled, and J_n and J_p are the current density for electrons and holes, respectively. Both α_n and α_p are strongly dependent on the electric field applied on the device and can be expressed as [25]

$$\alpha_{n,p} = \alpha^{\infty}{}_{n,p} \exp\left[-\left(\frac{E^{\text{crit}}{}_{n,p}}{E}\right)\right]. \quad (6)$$

Specifically, to calculate the impact ionization in the GaN wurtzite structure, the values of coefficients $\alpha_{n,p}$ and $E^{\text{crit}}_{n,p}$ were set to be 2.60×10^8 cm^{-1} and 3.42×10^7 V cm^{-1} for electrons, and 4.98×10^6 cm^{-1} and 1.95×10^7 V cm^{-1} for holes, respectively.

Results and discussion

Figure 2a shows a comparison of calculated conduction band profiles for all devices in the neutral bias condition. As observed on the conventional AlGaN/GaN HEMT (black solid line), the potential height toward the GaN buffer layer is insufficient to well confine the 2-DEG, and a spillover of transport electrons is hence expected under high-drain-voltage conditions. However, such phenomenon is alleviated in structures A to C, as a deeper and narrower potential well is formed to serve as the 2-DEG channel, providing a better confinement of transport electrons. Figure 2b plots the distribution of three-dimensional electron density (N_e) in a semi-log scale for all devices. Accordingly, N_e of structures A to C exhibits an almost identical distributed profile and have a similar peak value of $N_e = 4.24 \times 10^{18}$ cm^{-3}. Most importantly, introducing the EBL effectively reduces the spillover of transport electrons as the N_e (at depth = 0.04 μm) is remarkably decreased from $N_e = 7.21 \times 10^{16}$ cm^{-3} (the conventional HEMT) to $N_e = 1.48 \times 10^{11}$ cm^{-3} (structures A to C). Such orders-of-magnitude reduction in N_e indicates a significant enhancement of 2-DEG confinement beneficial from the employment of EBL structures. The origin of the above observations can be further illustrated by inspecting the corresponding distributed electric field (Figure 2c). For the conventional AlGaN/GaN HEMT, a negative electric field is induced in the 2-DEG channel (marked by the dotted-line rectangle) due to the accumulation of polarization charges supported by the $Al_{0.2}Ga_{0.8}N$ barrier layer. The electric field becomes positive in the region below the 2-DEG channel. Therefore, it is beneficial to repel the transport electrons toward the 2-DEG channel, confining them and preventing punchthrough. However, the magnitude of the electric field is generally too small to repel the spilling electrons in the conventional AlGaN/GaN HEMT structure. In contrast, the magnitude of the electric field is considerably enhanced by intentionally inserting the EBL into the HEMT, especially for structure C. Obviously, an extremely large electric field of $E = 350$ MV/cm is induced in structure C (at the bottom side of GaN channel layer, depth approximately 0.055 μm), which effectively depletes and confines the transport electrons into the 2-DEG channel, and that subsequently suppresses the subthreshold drain leakage current.

Figure 3a shows DC transfer characteristics, i.e., drain current (I_{ds}) versus gate voltage (V_g), of all devices in a semi-log scale with a drain voltage (V_{ds}) of $V_{ds} = 30$ V. At a given value of V_g, the conventional AlGaN/GaN HEMT always shows the largest subthreshold drain leakage current, and that is obviously decreased in structures A to C. While supplying a sufficiently high V_{ds} on the conventional AlGaN/GaN HEMT, the transport electrons can directly bypass the gate depletion region and drift into the GaN buffer layer underneath, increasing the subthreshold drain leakage current even under the threshold gate voltage (V_{th}) operation. Clearly, structure C exhibits the lowest subthreshold drain leakage current among all devices. It indicates that the transport electrons are effectively blocked by the AlGaN/GaN/AlGaN QW EBL and thus are not able to migrate via the buffer layer and contribute the leakage current. Figure 3b shows the subthreshold drain leakage versus drain voltage at a closed-gate condition below a threshold bias of $V_g = -5$ V for all devices. Here, the breakdown voltage (V_{br}) of the HEMT is defined as the voltage at which the subthreshold drain leakage current increases superlinearly with the drain voltage. The breakdown voltage identified for the conventional AlGaN/GaN HEMT, structure A, structure B, and structure C are $V_{br} = 48$ V, $V_{br} = 58$ V, $V_{br} = 115$ V, and $V_{br} = 285$ V, respectively. Restated, among all devices, a dramatic enhancement of V_{br} and a large reduction of subthreshold drain leakage current in structure C are mainly attributed to its improved confinement of transport electrons by the AlGaN/GaN/AlGaN QW EBL.

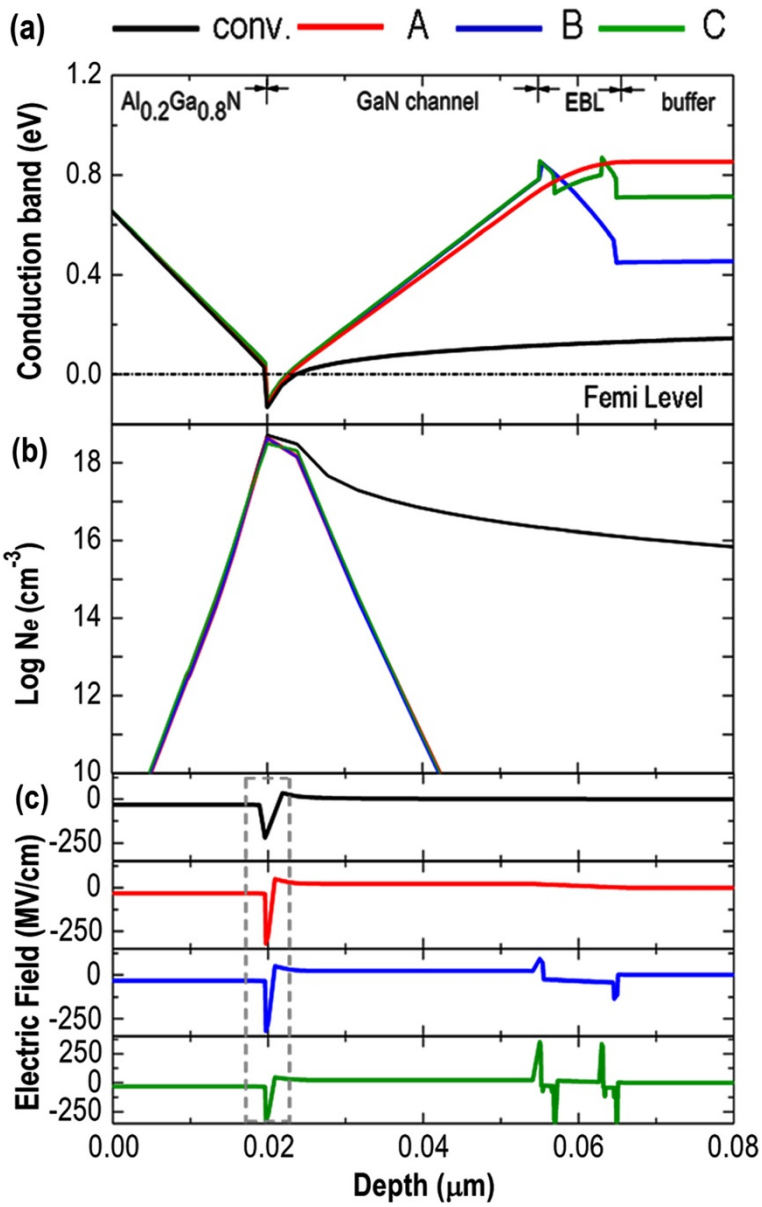

Figure 2 Conduction band, electron density, and electric field distribution versus depth plots. (a) Calculated conduction band profiles of all devices under the neutral bias condition. **(b)** Distribution of three-dimensional electron density (N_e) in a semi-log scale for all devices. **(c)** Corresponding electric field distributed over all devices. The dotted-line rectangle marks the region where the 2-DEG channel belongs.

Figure 4a plots cross sections of the electron concentration distribution at a closed-gate condition of $V_g = -5$ V and $V_{ds} = 80$ V for all devices. Obviously, the electrons under the gate electrode are depleted completely by the gate-induced electric field in the conventional AlGaN/GaN HEMT. Nevertheless, as the potential height provided by the GaN buffer layer is small, most of the transport electrons can still bypass this depletion region by migrating across the GaN buffer layer to the lower potential regions, causing an inevitable subthreshold drain leakage current. In structures A to C, the potential height (toward the GaN buffer layer) created by the EBL is increased, which prevents the transport electrons from spilling into the GaN buffer layer, reducing the HEMT's subthreshold drain leakage current. The functionality of EBL is further examined by inspecting the cross-sectional potential profiles for all devices under a closed-gate condition of $V_g = -5$ V with V_{ds} increasing from $V_{ds} = 20$ V to $V_{ds} = 60$ V in 20-V interval (Figure 4b). Accordingly, for the conventional AlGaN/GaN HEMT, there is already

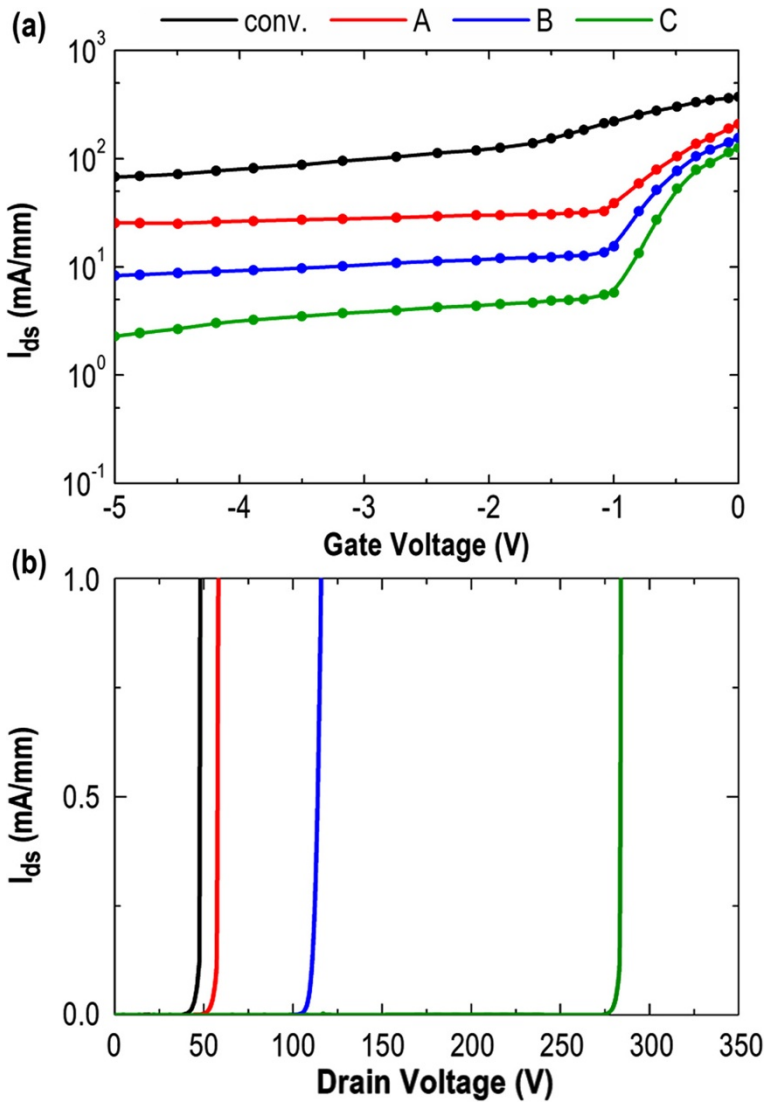

Figure 3 DC transfer characteristics and subthreshold drain leakage versus drain voltage plots. (a) Transfer characteristics (I_{ds} vs. V_g) for all devices with a drain voltage of $V_{ds} = 30$ V. **(b)** Subthreshold drain leakage current as a function of drain bias for all devices under a closed-gate condition of $V_g = -5$ V.

no potential barrier toward the GaN buffer layer even operating at the low drain bias of $V_{ds} = 20$ V. The situations become worse for the higher-drain-bias conditions of $V_{ds} = 40$ V and $V_{ds} = 60$ V. Thus, it is the main reason responsible for the smallest V_{br} of the conventional AlGaN/GaN HEMT. In contrast, introducing the EBL can raise the conduction band of the GaN channel layer by the bandgap difference, building a deeper potential well to confine 2-DEG, preventing punchthrough. Such effect is noticeable in structure C even when the HEMT is operated under a high-drain-bias condition. Additionally, due to the large electric field induced at the interfaces of AlGaN/GaN/AlGaN QW EBL, the potential decline of structure C in the conduction band (marked by the light-blue rectangle) with the increasing of V_{ds} is less pronounced, considerably postponing the device breakdown.

Figure 5a plots the 2-DEG density as a function of V_g for all devices. As compared to structures A to C, the conventional AlGaN/GaN HEMT has to be supplied with a much larger negative gate voltage to close the 2-DEG channel and diminish the 2-DEG density to a background value of approximately 10^2 cm^{-2}. Additionally, the estimated slope of the conventional AlGaN/GaN HEMT (i.e., the difference of 2-DEG density divided by the difference of V_g) is not as steep as that of structures A to C, suggesting a weak confinement of transport electrons. However, the 2-DEG density of

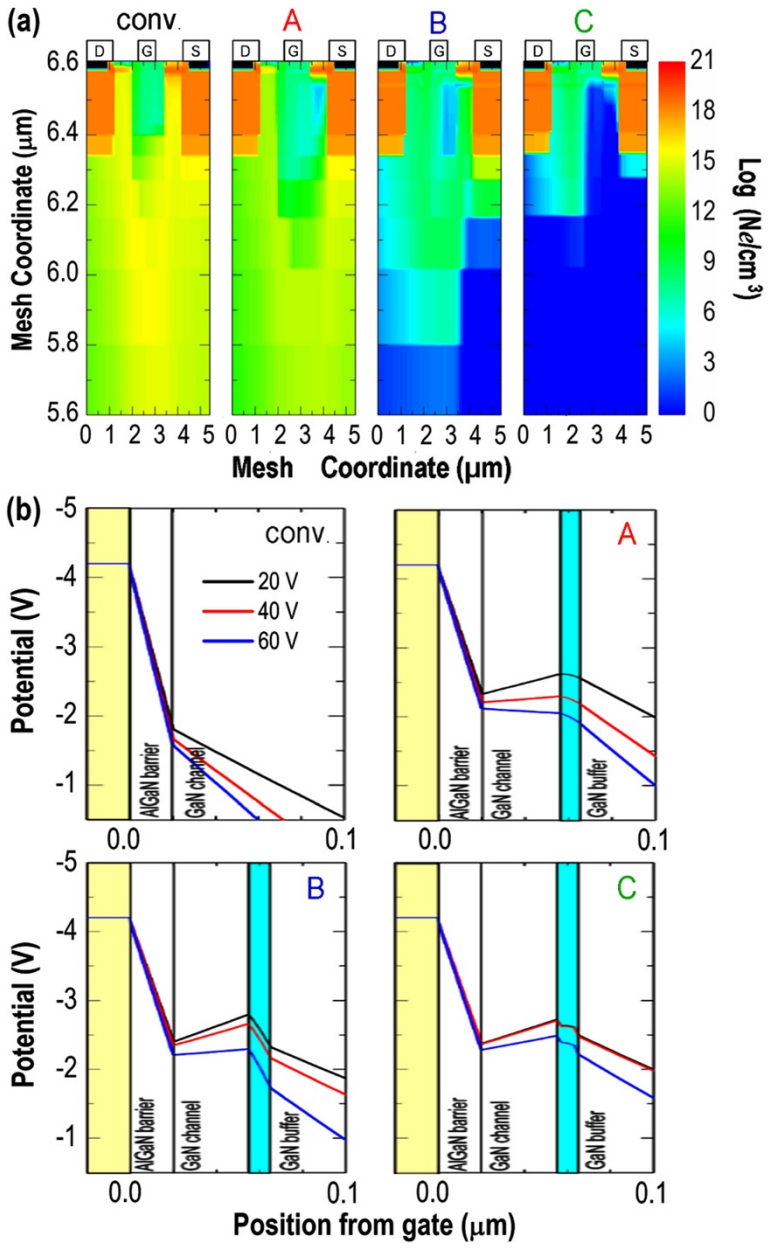

Figure 4 Cross sections of the electron concentration distribution at a closed-gate condition and cross-sectional potential profiles. (a) N_e distributions in all devices at a closed-gate condition of $V_g = -5$ V and $V_{ds} = 80$ V. **(b)** Cross-sectional potential profiles for all devices, where $V_g = -5$ V, $V_{ds} = 20$ V (black line), $V_{ds} = 40$ V (red line), and $V_{ds} = 60$ V (blue line). The EBL region is marked by the light-blue rectangle.

structures A to C increases rapidly at a low gate voltage (-1.25 V $\le V_g \le -0.50$ V), and that becomes saturated to approximately 10^{11} cm^{-2} at higher V_g. Figure 5b shows the 2-DEG mobility (μ) versus 2-DEG density for all devices. The 2-DEG mobility of all devices initially increases along with the increasing of 2-DEG density, primarily attributed to the enhancement of the screening effect against the ionized ion scattering [25-27]. Yet, the mobility degrading with the further increase of 2-DEG density is considered to be the result of electrons spilling into the AlGaN barrier layer [28-30]. Most importantly, structure C always exhibits the highest electron mobility and achieves a maximum value of $\mu = 940$ cm^2/V-s. Such high electron mobility is critical for the high-speed and high-power-switching applications.

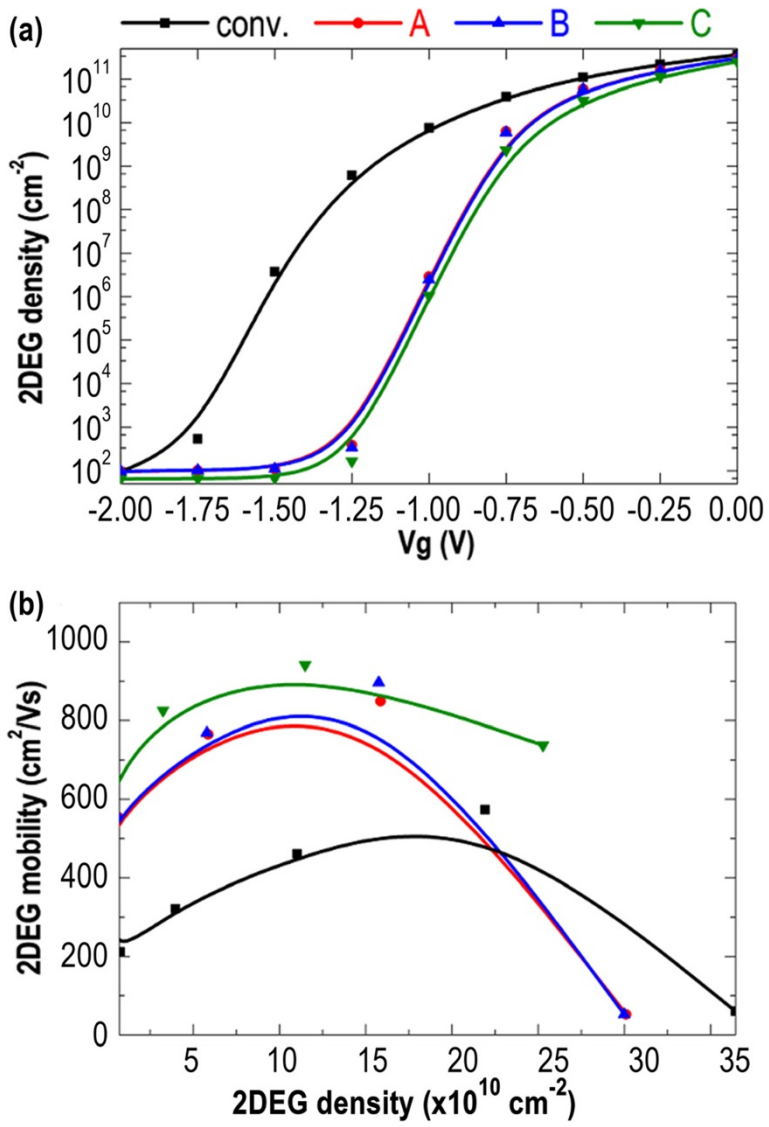

Figure 5 Dependence of 2-DEG density on gate voltage and 2-DEG mobility (μ) versus 2-DEG density plots. (a) Dependence of 2-DEG density on gate voltage (V_g) and **(b)** 2-DEG mobility (μ) versus 2-DEG density for all devices.

Finally, we are going to discuss the dependence of thickness and composition of QW EBL on the breakdown voltage of the HEMT. Figure 6a plots the breakdown voltage versus the GaN thickness of QW EBL, where the barrier layer of QW EBL is $Al_{0.1}Ga_{0.9}N$, and the total thickness of QW EBL is set to 10 nm. As compared to structure A (entire 10-nm-thick GaN EBL) and structure B (entire 10-nm-thick $Al_{0.1}Ga_{0.9}N$ EBL), introducing the QW EBL considerably enhances the breakdown voltage to a much higher level with an average value of V_{br} = 250 V. The ideal GaN thickness of QW EBL is around 4 to 6 nm, which provides a sufficient space to accommodate spilling electrons, prohibiting the further leakage of transport electrons into the GaN buffer layer. Figure 6b shows the dependence of aluminum composition of QW EBL on the breakdown voltage, where the GaN thickness is set to 6 nm, and the total thickness of QW EBL is again fixed to 10 nm. Clearly, the breakdown voltage only fluctuates slightly away from the line of V_{br} = 250 V while increasing the aluminum composition of the QW EBL from Al = 3% to Al = 20%, offering a greater tolerance for epitaxial imperfections during the fabrication of a AlGaN/GaN/AlGaN QW EBL structure.

Conclusions

In conclusion, we propose a novel AlGaN/GaN/AlGaN QW EBL structure to alleviate the punchthrough effect that is generally observed on the conventional AlGaN/

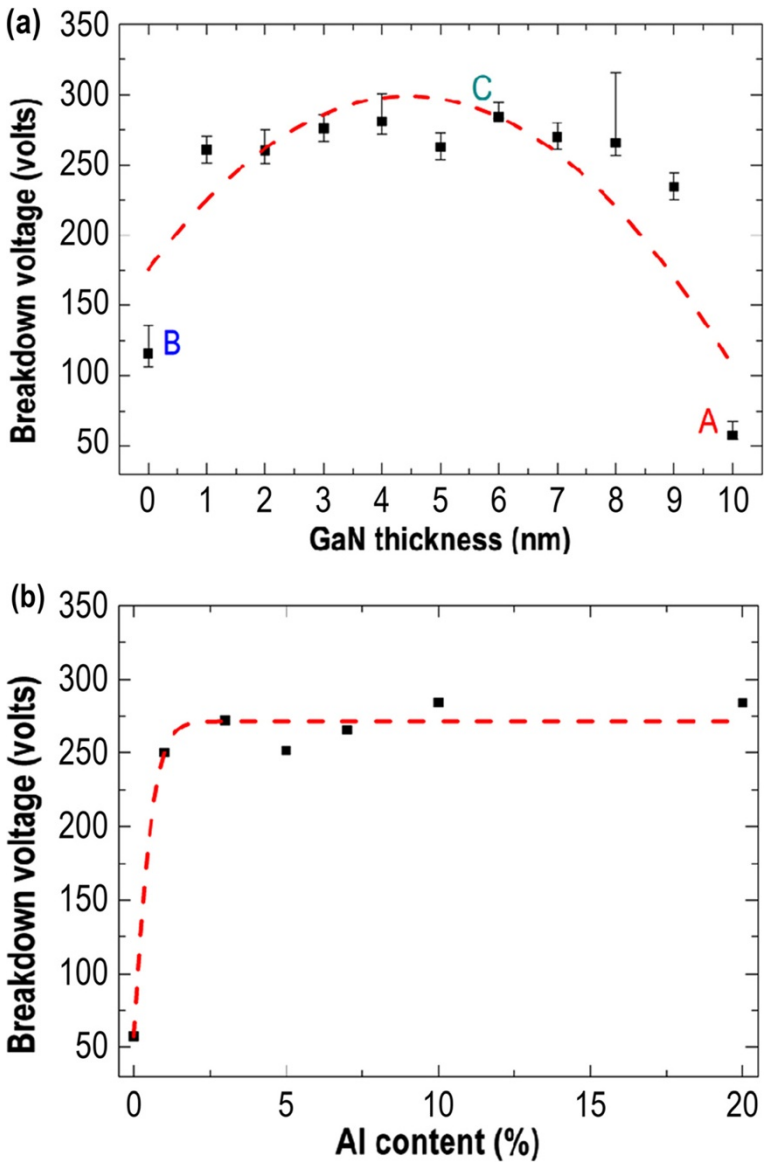

Figure 6 Breakdown voltage versus GaN thickness and dependence of aluminum composition on breakdown voltage. (a) HEMT's breakdown voltage versus the GaN thickness of QW EBL, where the barrier layer of QW EBL is $Al_{0.1}Ga_{0.9}N$ and the total thickness of QW EBL is set to 10 nm. **(b)** Dependence of aluminum composition of QW EBL on the HEMT's breakdown voltage, where the GaN thickness of QW EBL is set to 6 nm and the total thickness of QW EBL is again fixed to 10 nm.

GaN HEMT. The introduction of AlGaN/GaN/AlGaN QW EBL leads to a better confinement of transport electrons into the 2-DEG channel, resulting in a reduction of subthreshold drain leakage current and a postponement of device breakdown. The large electric field induced at the interfaces of AlGaN/GaN/AlGaN QW EBL, which effectively depletes the spilling electrons toward the 2-DEG channel, is mainly responsible for the improved performances.

Competing interests

The authors declare that they have no competing interests.

Authors' contributions

Y-CY, L-LC, and C-YL carried out the simulation program and participated in the design of the study. C-YH and T-YL carried out the calculation and helped to draft the manuscript. M-TW and J-MH participated in the design of the study. Y-JL conceived the study and participated in its design and coordination and helped to draft the manuscript. All authors read and approved the final manuscript.

Acknowledgements

The authors gratefully acknowledge financial support from the National Science Council of the Republic of China (ROC) in Taiwan (contract no. NSC–100–2112–M–003–006–MY3), from the Bureau of Energy, Ministry of Economic Affairs in Taiwan, and from the Ministry of Science and Technology in Taiwan (contract no. MOST 103–2112–M–003–008–MY3).

Author details
[1]Institute of Electro-Optical Science and Technology, National Taiwan Normal University, 88, Sec. 4, Ting-Chou Road, Taipei 116, Taiwan. [2]Institute of Electronics Engineering, National Taiwan University, 1, Sec. 4, Roosevelt Road, Taipei 106, Taiwan. [3]Institute of Optoelectronic Sciences, National Taiwan Ocean University, 2, Pei-Ning Road, Keelung 202, Taiwan. [4]Solid-State Lighting Systems Department, Green Energy and Environment Research Laboratories, Industrial Technology Research Institute (ITRI), Hsinchu 310, Taiwan.

Received: 6 June 2014 Accepted: 19 August 2014
Published: 27 August 2014

References

1. Mustafa F, Hashim AM: **Generalized 3D transverse magnetic mode method for analysis of interaction between drifting plasma waves in 2DEG-structured semiconductors and electromagnetic space harmonic waves.** *Prog Electromagn Res* 2010, **102:**315–335.
2. Park PS, Nath DN, Krishnamoorthy S, Rajan S: **Electron gas dimensionality engineering in AlGaN/GaN high electron mobility transistors using polarization.** *Appl Phys Lett* 2012, **100:**063507.
3. Saito W, Takada Y, Kuraguchi M, Tsuda K, Omura I, Ogura T, Ohashi H: **High breakdown voltage AlGaN-GaN power-HEMT design and high current density switching behavior.** *IEEE Trans Electron Devices* 2003, **50:**2528–2531.
4. Saito W, Omura I, Ogura T, Ohashi H: **Theoretical limit estimation of lateral wide band-gap semiconductor power-switching device.** *Solid State Electron* 2004, **48:**1555–1562.
5. Cho E, Brunner F, Zhytnytska R, Kotara P, Würfl J, Weyers M: **Enhancement of channel conductivity in AlGaN/GaN heterostructure field effect transistors by AlGaN:Si back barrier.** *Appl Phys Lett* 2011, **99:**103505.
6. Bahat-Treidel E, Brunner F, Hilt O, Cho E, Wurfl J, Trankle G: **AlGaN/GaN/GaN:C back-barrier HFETs with breakdown voltage of over 1 kV and low $R_{ON} \times A$.** *IEEE Trans Electron Devices* 2010, **57:**3050–3058.
7. Xu Y, Guo Y, Xia L, Wu Y: **An support vector regression based nonlinear modeling method for SiC MESFET.** *Prog Electromagn Res* 2008, **2:**103–114.
8. Lee YJ, Yang ZP, Lo FY, Siao JJ, Xie ZH, Chuang YL, Lin TY, Sheu JK: **Slanted n-ZnO/p-GaN nanorod arrays light-emitting diodes grown by oblique-angle deposition.** *APL Mater* 2014, **2:**056101.
9. Sun HH, Guo FY, Li DY, Wang L, Wang DB, Zhao LC: **Intersubband absorption properties of high Al content Al(x)Ga(1 – x)N/GaN multiple quantum wells grown with different interlayers by metal organic chemical vapor deposition.** *Nanoscale Res Lett* 2012, **7:**649.
10. Brunner F, Bahat-Treidel E, Cho M, Netzel C, Hilt O, Würfl J, Weyers M: **Comparative study of buffer designs for high breakdown voltage AlGaNGaN HFETs.** *Phys Status Solidi C* 2011, **8:**2427–2429.
11. Sadahiro K, Yoshihiro S, Hitoshi S, Iwami M, Seikoh Y: **C-doped GaN buffer layers with high breakdown voltages for high-power operation AlGaN/GaN HFETs on 4-in Si substrates by MOVPE.** *J Cryst Growth* 2007, **298:**831–834.
12. Choi YC, Pophristic M, Peres B, Cha H-Y, Spencer MG, Eastman LF: **High breakdown voltage C-doped GaN-on-sapphire HFETs with a low specific on-resistance.** *Semicond Sci Technol* 2007, **22:**517–521.
13. Bahat-Treidel E, Hilt O, Brunner F, Wurfl J, Trankle G: **Punchthrough-voltage enhancement of AlGaN/GaN HEMTs using AlGaN double-heterojunction confinement.** *IEEE Trans Electron Devices* 2008, **55:**3354–3358.
14. Xu PQ, Jiang Y, Chen Y, Ma ZG, Wang XL, Deng Z, Li Y, Jia HQ, Wang WX, Chen H: **Analyses of 2-DEG characteristics in GaN HEMT with AlN/GaN super-lattice as barrier layer grown by MOCVD.** *Nanoscale Res Lett* 2012, **7:**141.
15. Bahat-Treidel E, Hilt O, Brunner F, Sidorov V, Wurfl J, Trankle G: **AlGaN/GaN/AlGaN DH-HEMTs breakdown voltage enhancement using multiple grating field plates (MGFPs).** *IEEE Trans Electron Devices* 2010, **57:**1208–1216.
16. Brown GF, Ager JW, Walukiewicz W, Wu J: **Finite element simulations of compositionally graded InGaN solar cells.** *Sol Energ Mat Sol C* 2010, **94:**478–483.
17. Bergman L, Chen X, McIlroy D, Davis RF: **Probing the $Al_xGa_{1-x}N$ spatial alloy fluctuation via UV-photoluminescence and Raman at submicron scale.** *Appl Phys Lett* 2002, **81:**4186–4188.
18. Yao YC, Tsai MT, Huang CY, Lin TY, Sheu JK, Lee YJ: **Efficient collection of photogenerated carriers by Inserting double tunnel junctions in III-nitride p-i-n solar cells.** *Appl Phys Lett* 2013, **103:**193503.
19. Kladko V, Kuchuk A, Lytvyn P, Yefanov O, Safriuk N, Belyaev A, Mazur YI, DeCuir EA Jr, Ware ME, Salamo GJ: **Substrate effects on the strain relaxation in GaN/AlN short-period superlattices.** *Nanoscale Res Lett* 2012, **7:**289.
20. Emami SD, Hajireza P, Abd-Rahman F, Abdul-Rashid HA, Ahmad H, Harun SW: **Wide-band hybrid amplifier operating in S-band region.** *Prog Electromagn Res* 2010, **102:**301–313.
21. Ambacher O, Foutz B, Smart J, Shealy JR, Weimann NG: **Two dimensional electron gases induced by spontaneous and piezoelectric polarization in undoped and doped AlGaN/GaN heterostructures.** *J Appl Phys* 2000, **87:**334–344.
22. Domen K, Horino K, Kuramata A, Tanahashi T: **Analysis of polarization anisotropy along the c axis in the photoluminescence of wurtzite GaN.** *Appl Phys Lett* 1997, **71:**1996–1998.
23. Rau B, Waltereit P, Brandt O, Ramsteiner M, Ploog KH, Puls J, Henneberger F: **In-plane polarization anisotropy of the spontaneous emission of M-plane GaN/(Al, Ga)N quantum wells.** *Appl Phys Lett* 2000, **77:**3343–3345.
24. Hu WD, Chen XS, Quan ZJ, Zhang XM, Huang Y, Xia CS, Lu W, Ye PD: **Simulation and optimization of GaN-based metal-oxide-semiconductor high-electron-mobility-transistor using field-dependent drift velocity model.** *J Appl Phys* 2007, **102:**034502-1–034502-7.
25. Oubram O, Gaggero-Sager LM, Bassam A, Luna Acosta GA: **Transport and electronic properties of two dimensional electron gas in delta-migfet in GaAs.** *Prog Electromagn Res* 2010, **110:**59–80.
26. Maeda N, Saitoh T, Tsubaki K, Nishida T, Kobayashi N: **Two-dimensional electron gas transport properties in AlGaN/GaN single- and double-heterostructure field effect transistors.** *Mater Sci Eng B* 2001, **82:**232–237.
27. Maeda N, Saitoh T, Tsubaki K, Nishida T, Kobayashi N: **Enhanced effect of polarization on electron transport properties in AlGaN/GaN double-heterostructure field-effect transistors.** *Appl Phys Lett* 2000, **76:**3118–3120.
28. Acar S, Lisesivdin SB, Kasap M, Ozcelik S, Ozbay E: **Determination of two-dimensional electron and hole gas carriers in AlGaN/GaN/AlN heterostructures grown by metal organic chemical vapor deposition.** *Thin Solid Films* 2008, **516:**2041–2044.
29. Chaibi M, Fernande T, Mimouni A, Rodriguez-Tellez J, Tazon A, Mediavilla Sanchez A: **Nonlinear modeling of trapping and thermal effects on GaAs and GaN MESFET/HEMT devices.** *Prog Electromagn Res* 2012, **124:**163–186.
30. Sang L, Schutt-Aine JE: **An improved nonlinear current model for GaN HEMT high power amplifier with large gate periphery.** *J Electromagnet Wave* 2012, **26:**284–293.

doi:10.1186/1556-276X-9-433
Cite this article as: Lee *et al.*: High breakdown voltage in AlGaN/GaN HEMTs using AlGaN/GaN/AlGaN quantum-well electron-blocking layers. *Nanoscale Research Letters* 2014 **9**:433.